The International Supercritical CO_2 Energy Technologies Symposium
March 2 - 5, 2026, Pittsburgh, PA
Paper #046

Design and Analysis of a 25 MWe Supercritical CO2 Turbo Machine

Amin Changizi
Senior Engineer
GE Vernova Advanced Research
Niskayuna, NY

Sylvain Pierre
Senior Engineer
GE Vernova Advanced Research
Niskayuna, NY

Yuankang Chen
Lead Engineer
GE Vernova Advanced Research
Niskayuna, NY

Dan Bacellar
Lead Engineer
GE Vernova Advanced Research
Niskayuna, NY

Thomas Mancuso
Senior Engineer
GE Vernova Advanced Research
Niskayuna, NY

ABSTRACT

This paper presents the design and analysis of a turbo machine operating with supercritical carbon dioxide (sCO2) in a 25 MWe Recompression Brayton Cycle (RCBC). The work was performed under US Department of Energy (DoE) program DE-EE-0010318. The design process involves the aerodynamic design of the compressor and turbine, including the initial layout of flowpaths and stage configurations to achieve high efficiency and performance. Additionally, a comprehensive rotodynamic analysis is performed to ensure the stability and reliability of the system. Conceptual designs for a high-speed motor and synchronous generator that match turbomachinery requirements are also developed from first principles.

1. INTRODUCTION

GE Vernova Advanced Research and its partners have been an integral part of the DOE-funded decade-long research effort to develop and commercialize sCO2-based turbomachinery [1, 2, 3, 4, 5, 6, 7, 8, 9, 10] [11] using recompression closed Brayton cycle (RCBC) for solar-, fossil-, and nuclear-based power generation.

The work reported in this paper was performed under DOE contract DE-EE0010318. GE Vernova Advanced Research in collaboration with Southwest Research Institute (SwRI) and Sandia National Laboratory delivered an initial conceptual design of a supercritical carbon dioxide (sCO2) power block for Gen3/Gen3++ [12] concentrated solar power (CSP) applications towards a levelized cost of electricity (LCOE) of $0.05/kWhr [13]. This is the first step towards the program objective of designing a preliminary integrated CSP plant based on an in-depth techno-economics LCOE analysis.

Part of the work scope includes a preliminary design of the power block comprising novel turbomachinery layouts, electrical motor and generator, along with practical aspects of the power block design such as the plant piping layout and inventory management system; an initial configuration of the solid-particle based thermal system including the heliostat field, particle thermal storage system, conveyance system, particle-based primary heat exchanger, and the

solar receiver.

This paper covers the initial turbomachinery design used for the cost model as well as the rotodynamic feasibility. In the initial phase of the study, a 25 MWe plant configuration based on a Recompression Brayton Cycle (RCBC) with a turbine inlet temperature of 600°C was selected. The conceptual design of the turbomachinery is presented in the following sections.

2. RESULTS AND DISCUSSION

2.1 Power Block

The conceptual analysis of the cycle was done in ASPEN Plus [14] and shown in Figure 1. The cycle configuration is a recompression Brayton cycle (RCBC), with a main compressor (MC) operating near the critical point of CO2 at 35 °C, a recompressor (RC) in parallel at a higher inlet temperature. The compressors are coupled with a high temperature turbine (HTT): together, these will be referred to as the high turbine spool; the speed of rotation was set to 17,000 rpm for the study.

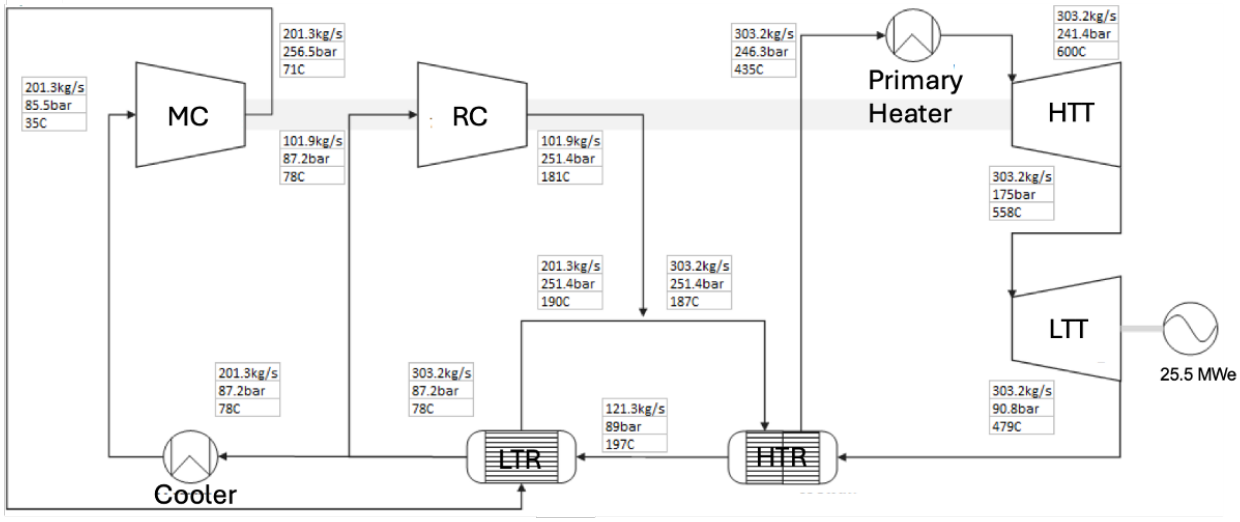

Figure 1 Cycle Conditions Used for the Initial Turbomachinery Layout

The flowpath of the high turbine spool continues to a low temperature turbine (LTT) connected to a generator synchronized to the grid. The LTT produces 25.5 MWe.

2.2 Turbomachinery Aerodynamic Design

The aerodynamic meanline tool used to layout the flowpath was done using an in-house code for the turbines, and Concept NREC's COMPAL® [15] for the compressors. Both tools incorporate the use of equilibrium real gas tables based on REFPROP [16] for the thermodynamic state calculation. The outcome of this initial study are flow path geometries (radii, blade heights, axial spacing, stage counts) of the turbines and compressors which are used for rotodynamic feasibility. The geometrical definitions below are considered preliminary and

unoptimized, however sufficient for the purpose of the reported study.

The main compressor and re-compressor geometry is summarized in Figure 2. MC consists of 2 shrouded impellers, with radial inlet guide vanes (IGV), vaneless diffusers, return channel and exit scroll. RC consists of 3 shrouded impellers, with radial IGV, vaneless diffusers, return channels and exit scroll.

For the HTT, a 2-stage turbine was selected, as shown in Figure 3. For the LTT, a 10-stage turbine with selected following a sensitivity study with the number of stages, as shown in Figure 4. The HTT is sized to produce the power required to turn the compressors.

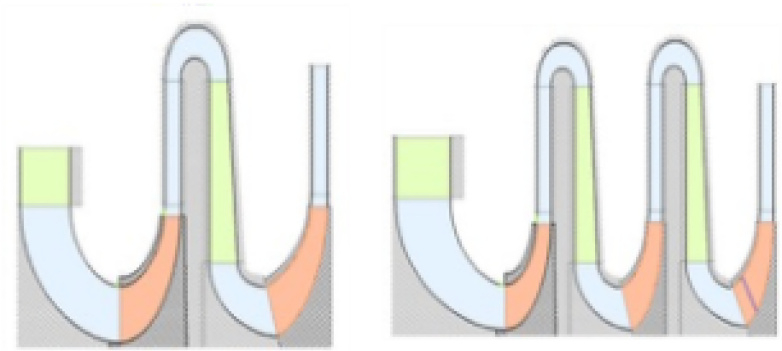

Figure 2: Compressors Layout

Figure 3:Four point of High Temperature Turbine Layout

Figure 4: For point of Low Temperature Turbine Layouts

2.4 ELECTRIC MACHINE DESIGN

The two electric machines are used in the power cycle: a high-speed motor to assist the start-up of the HTT; and a 25 MWe synchronous generator connected to grid. Hermetic and non-hermetic options for both machines have been sized via first principles, and the cost estimated with a Bill of Materials (BOM) supported by engineering estimates. For the rotodynamic analysis however, only the hermetic design is reported.

2.4.1 Hermetic vs non-hermetic – general considerations

The electric machines operating in the supercritical CO_2 cycle can be either hermetic or non-

hermetic, with critical tradeoffs to be considered between.

Having non-hermetic machines on the same shaft as the turbomachinery means complex seals around the shaft are required to minimize leakage of CO_2 into the environment. Any leakage flow is a release of a greenhouse gas, represents lost work and heat from the cycle, and requires plant operators to regularly top up the system to replenish the working fluid lost to leaks.

However, hermetic machines also have many challenges to be addressed. A hermetic electric machine must be protected against the risk of corrosion resulting from exposure to supercritical CO_2 [20]. The winding insulation can be protected by canning, where the stator or rotor that contains the windings are encapsulated in a protective shell. This shell will be constructed of a metal resistant to carbonic acid, except in the air gap between rotor and stator where the changing electric fields produce large eddy current losses in the metal casing. There, a carbon fiber composite (CFRP) would be preferred instead, although literature suggests the CFRP matrix is vulnerable to carbonic acid damage as it is very difficult to ensure there is zero moisture in CO2 used in the cycle. The canning material in the air gap must be carefully evaluated during the detailed design phase of a hermetic machine.

Hermetic operation of the electric machine also means the fluid in the stator-rotor air gap is of comparable density and temperature to that of the nearby turbomachinery component. This results in windage losses that are significantly higher than if the electric machine was operated in ambient air conditions and our estimates below show that the windage losses are typically the dominant machine loss for hermetic machines. As windage loss scales with tip radius to the fourth power [21], it is possible to reduce the windage loss substantially by reducing the rotor tip radius and increasing the machine length. Reducing tip radius, however, comes at the cost of some combination of increased electromagnetic (and hence thermal) loading and a larger and longer machine. Table 1 below shows the tradeoff between the windage loss and BOM cost for a hermetic 25 MWe synchronous generator with the mechanical speed and electromagnetic and thermal loading held constant. The optimal hermetic electric machine design is thus likely different from a non-hermetic one due to the differing cost and performance constraints.

Table 1: Tradeoff Between Cost and Windage Loss for a Hermetic 25MWe Generator

Design	Rotor L/D	%Windage loss	%BOM Cost
Nominal Diameter	1.49	100%	100%
90% Diameter	2.05	81%	98%
80% Diameter	2.92	64%	100%
70% Diameter	4.36	49%	104%

2.4.2 25 MWe Synchronous Generator – Design and Costing

The hermetic synchronous generator has a rotor-stator air gap assumed to be filled with sCO_2 at the LTT inlet condition. The thermal shield will cool the CO_2 from the turbine side that flows into the generator cavity to allow for acceptable temperature for the stator insulation winding. Table 2 details the key parameters of the generator under nominal operating conditions. This design can also be used for the non-hermetic option (with the canning removed), or an off-the-shelf 25 MWe generator could be used instead.

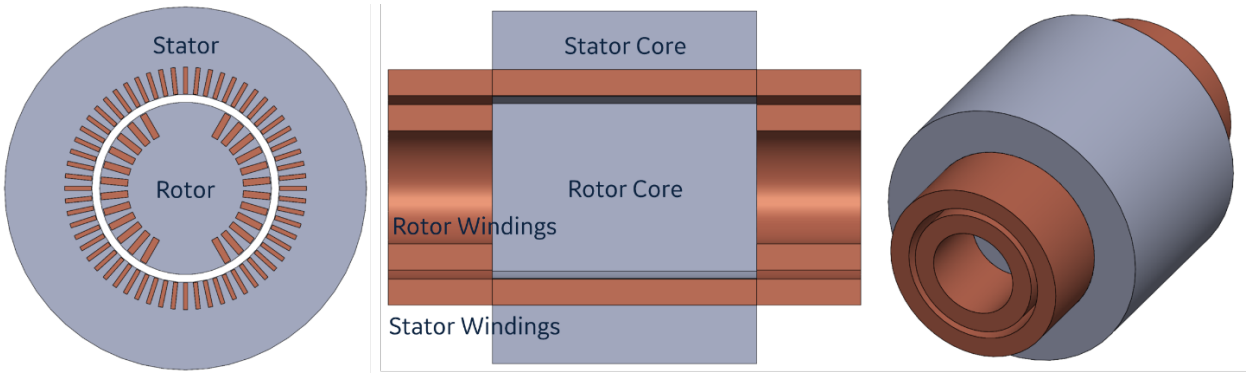

Figure 5: Conceptual Layout of a 25 MWe Synchronous Generator

Table 2: 25 MWe Hermetic Synchronous Generator – Nominal Parameters

Parameter	Value	Unit
Rated Power	25	MW
Speed	3600	RPM
Torque	66315	Nm
Power Factor	0.9	-
Electrical Frequency	60	Hz
Line-Line Voltage, RMS	13800	V

2.4.2 High-Speed Motor – Design and Cost

The motor on the high-speed spool is sized for cycle startup condition, rotates at 17,000 rpm (see Figure 6). The design for the hermetic and non-hermetic options is similar – both are Permanent Magnet (PM) machines, with NdFeB magnets arranged in a Halbach Array configuration secured to the rotor by a carbon fiber wrap. The PM architecture was selected as they enabled relatively large air gaps (critical to keeping windage losses low) and produce lower losses in the rotor (making them easier to cool). The motors have a power factor of unity and are driven by fully rated AC-AC converters connected to the grid with an assumed 98% conversion efficiency. These converters comprise approximately 80% of the cost of the motor drive and scale directly with the rated power providing strong motivation to reduce the startup power requirements.

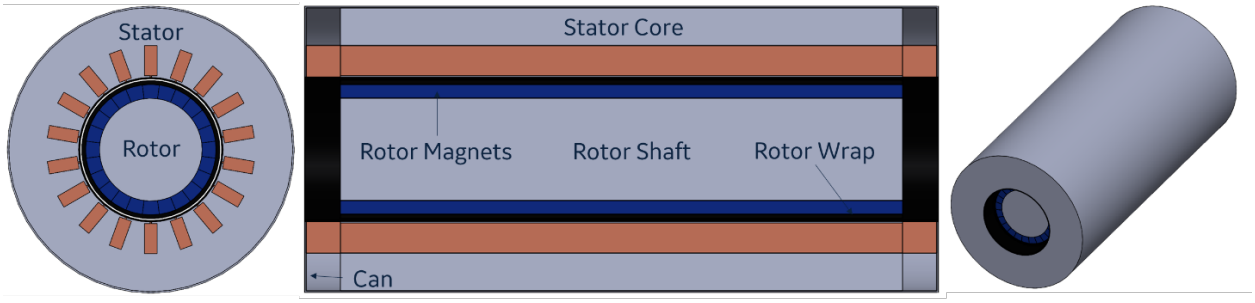

Figure 6: Conceptual Layout of the Hermetic Motor

A key consideration for this application is that the motor is continually producing windage and core losses while the shaft is spinning, even while the machine is unpowered. One possible option to mitigate this loss is to include a clutch that disengages the motor from the high-speed spool after startup, represented as one of the rotordynamic configurations assessed later in the paper.

The hermetic motor is assumed to operate in gaseous CO_2 attained with a combination of a low-leakage seal between the generator and compressor and a pressure management system that pumps the gas out of the generator cavity [11]. This management system is necessary as operating the generator to compressor inlet conditions would result in windage losses larger than the rated power of the motor itself. However, this leakage flow must then be recompressed and returned to the cycle, representing additional losses currently not accounted for.

The non-hermetic motor is assumed to operate in ambient air conditions. It would have a larger tip radius due to the reduced windage loss, allowing for a less bulky machine with a shortened rotor and slightly reduced core losses. Both hermetic and non-hermetic designs have similar cost, as the bulk of the cost comes from the AC-AC drive (which would be identical in both).

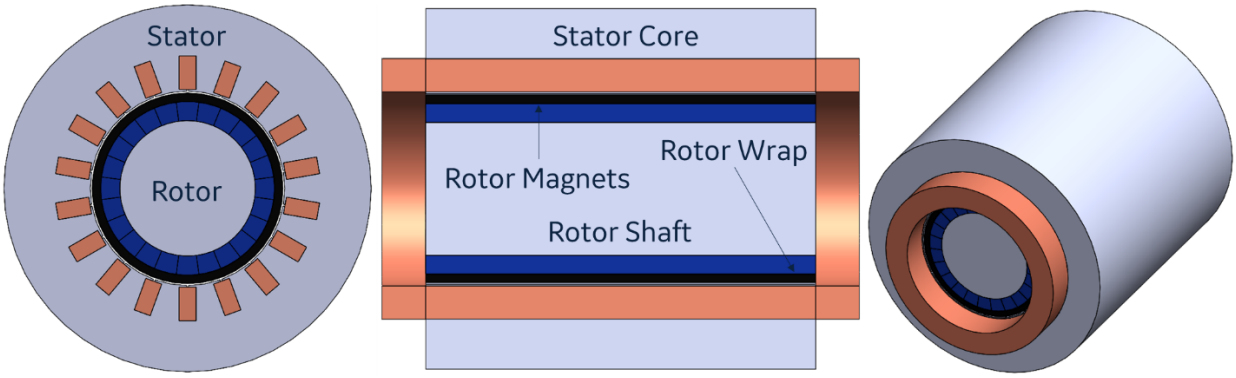

Figure 7: Conceptual Layout of the Non-Hermetic Motor

2.5 MECHANICAL ROTOR TRAIN EVALUATION

2.5.1 Overview

Following the completion of the initial conceptual aerodynamic design for the compressors,

turbines and electric motors and generators, a rotor train study of configuration layouts (with hermetic machines) with corresponding rotodynamic analysis was conducted.

In laying out the options, two primary objectives were identified: first, to avoid operating the entire turbo machine near its critical speed; and second, to separate and isolate hot surface areas from those that should operate at lower temperatures. Only the HTT evaluation is presented, which has a rotational speed of 17,000 rpm. Furthermore, the layout assumes the compressor thrust force is set opposite to the turbine to size the balance piston.

2.5.2 Configuration designs

Five configurations were proposed, which are illustrated in Figure 8 to 13.

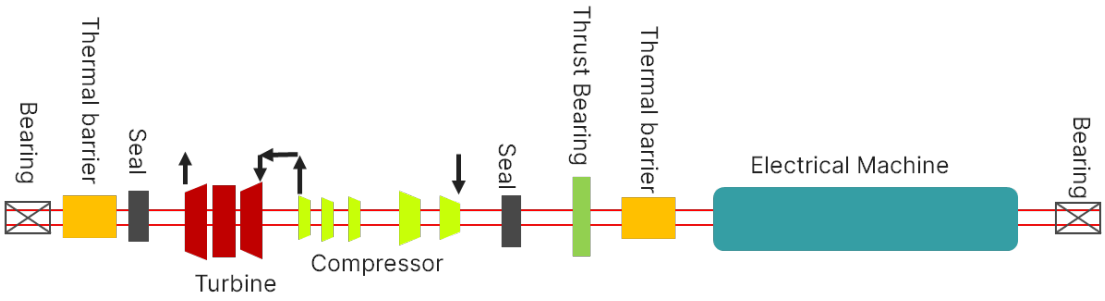

Figure 8. Rotor Train Configuration 1

The first configuration, illustrated in Figure 8, features the entire system supported between two bearings. To isolate the bearings and electrical machine from high temperatures, thermal barriers are employed. However, the seals and thrust bearing are still exposed to high temperatures due to their proximity to the turbine and compressor.

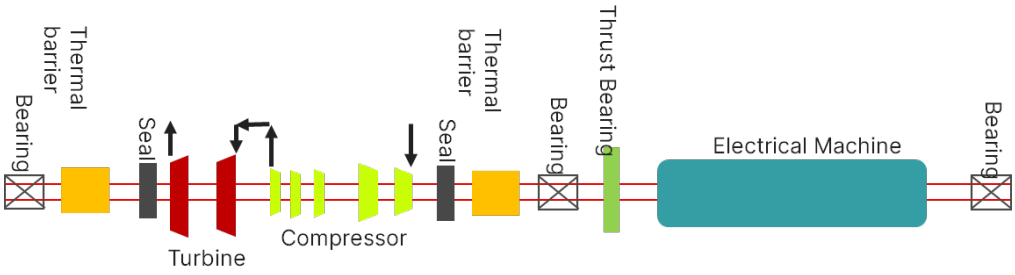

Figure 9. Rotor Train Configuration 2

Figure 9 illustrates the second possible configuration for the system. In this design, an additional bearing is added to the system to help control vibration and critical speed. Furthermore, the thermal barriers are utilized to protect the thrust bearing, providing improved thermal isolation compared to the first design.

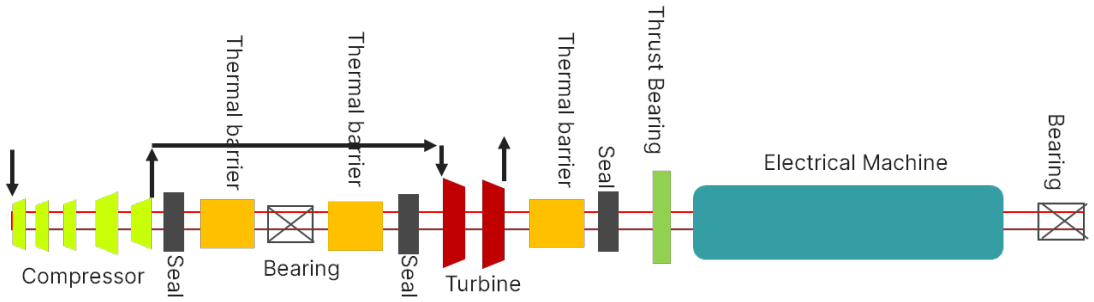

Figure 10. Rotor Train Configuration 3

Figure 10 shows the third configuration, which features an overhung compressor design. This design facilitates easier assembly and manufacturing of the system, while also providing better protection for the bearings. Additionally, three thermal barriers and an extra seal are employed to mitigate the effects of high pressure. In this configuration, the thrust bearing and electrical machine are located on the cold side of the system, which provides improved thermal isolation. However, the notable drawback of this design is having the compressor overhung, which can reduce the critical speed of the system and have an adverse impact on compressor clearances.

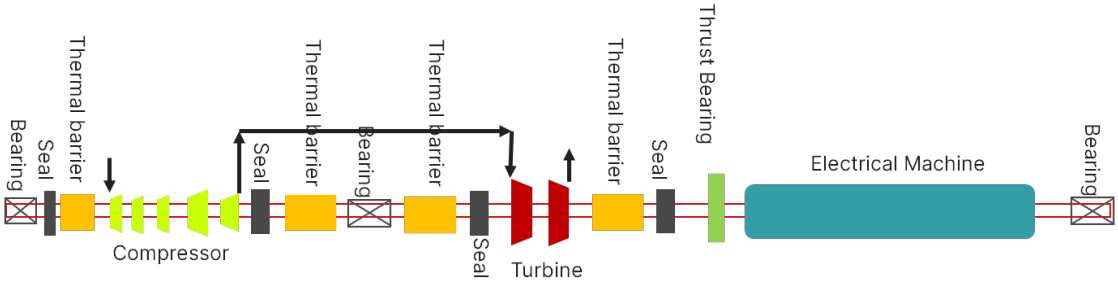

Figure 11. Rotor Train Configuration 4

The fourth design, Figure 11, addresses the issue of reduced critical speed due to the overhung compressor (configuration 3) by adding an additional bearing at the end of the shaft. This design features four thermal barriers to protect the bearings and multiple seals from high temperatures. This configuration provides improved thermal isolation and reduces thermal stress on the components.

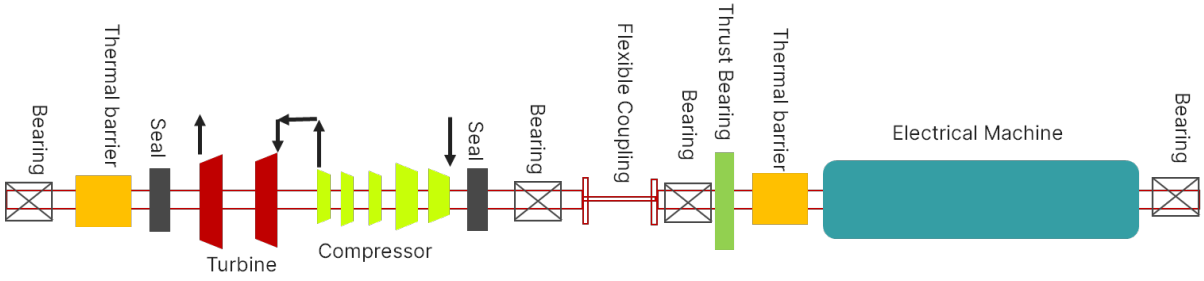

Figure 12. Rotor Train Configuration 5

The last option configuration considered has the electrical machine separated from the turbo

machine, with the two shafts connected by a flexible coupling, as shown in Figure 12. This design includes two thrust bearings to control the thrust load, with each shaft supported by two bearings, resulting in a total of four bearings. This represents twice the number of bearings compared to the other designs and double the number of thrust bearings.

For all the designs considered, it is assumed that the entire system would be hermetically sealed. This would enable the prevention of leakage to the outside of the system, thereby maintaining a sealed environment and minimizing potential losses or contamination.

Finally, in terms of axial thrust management, the installation direction of the compressor and re-compressor are opposite to that of the turbine. Balance pistons and thrust bearings have been incorporated on both sides of the system. The purpose of the balance piston is to reduce the thrust load on the thrust bearing. Dry gas seals are used to mitigate CO2 pressure on the generator or bearings.

2.5.2 Rotodynamic Analysis

The evaluation of the four configurations followed American Petroleum Institute (API) 617 and API 584, with the criterion of having 10% margin at design operating speed.

For each configuration, a finite element model was developed in Dyrobes [22], and the critical speeds were swept across the design space, and results extracted for calculated stiffness values of 10^6 and 10^7 to obtain the sensitivity on the critical speeds of the system as shown in Figure 13 & Figure 14. An example of such finite element is shown in Figure 15 for configuration 3.

When the bearing stiffness is around 10^6, configurations 1 and 2 have Mode 3 critical speed that falls within or close to 10% of the operating point, while Configuration 5 has both Mode 3 and 4 critical speeds within this range. For a bearing stiffness of 10^7, configurations 1 and 4 have a Mode 3 critical speed close to 10% of the operating point, and Configuration 2 has a Mode 2 critical speed within this range.

At first glance, configuration 1 closely straddles the speed avoidance zone, configuration 2 would require lowering its system stiffness to avoid a crossing, configuration 3 (overhung) & 4 (3 bearings) have good separation at lower bearing stiffness while straddling the limit at the higher bearing stiffness. Learning of configuration 2 implies needing a bearing between the compressor and the turbine when the second bearing is located near the electric motor. Configuration 5 has mode 3 and 4 crossings at the lower stiffness and would require increasing its system stiffness. From the above discussions, configurations 1 and 4 appear best suited for future development.

It is also important to consider that these findings are based on the minimum shaft diameter for torque transmission. If the shaft diameter is increased, the system's stiffness and critical speed will likely change

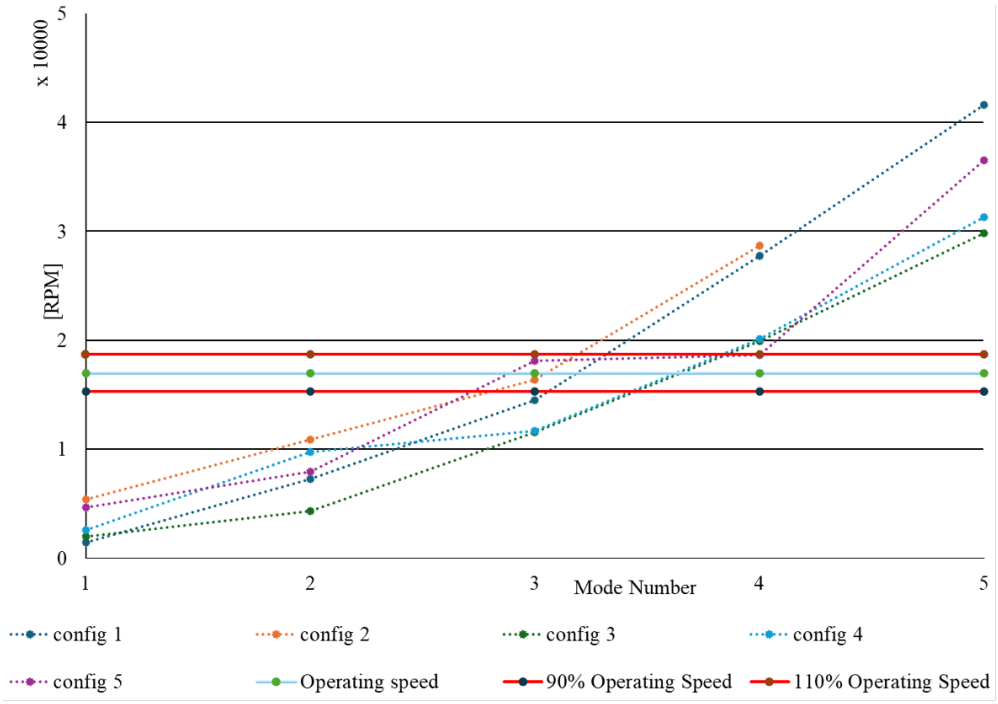

Figure 13. Critical Speed of Different Configurations with Bearing Stiffness of 10^6

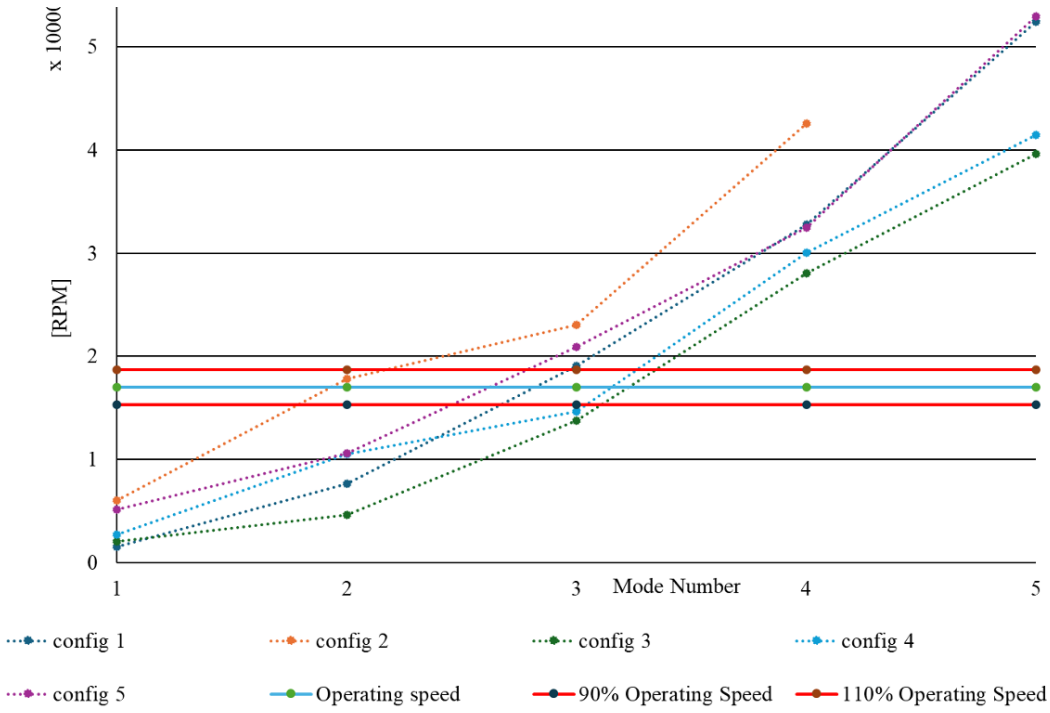

Figure 14. Critical Speed of Different Configurations with Bearing Stiffness of 10^7

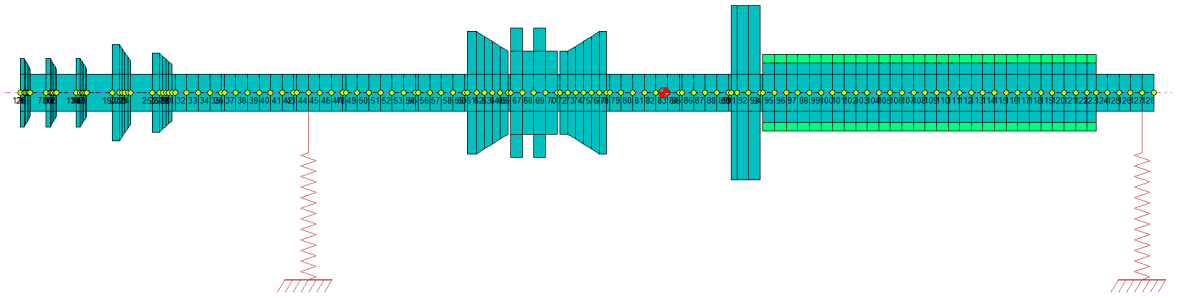

Figure 15. FE Model of Configuration 3

CONCLUSION

An initial conceptual flowpath and rotor trains with compressors, turbines, motor and generator was developed for a cascaded CSP RCBC cycle with turbine inlet temperature of 600ºC producing 25 MWe when connected to the grid. The study is part of an effort to develop and optimize techno-economics models for a CSP plant towards the LCOE goal of $0.05/kWh. The turbomachinery system was split into a high turbine spool with a 2-stage main compressor, 3-stage re-compressor and 2-stage turbine in a RCBC arrangement on a common rotor train; which flowpath was then cascaded into a low temperature turbine connected to a generator synchronized to the grid. Hermetic and non-hermetic electric motors and generators were evaluated. For this study, the high temperature spool was evaluated for five possible rotor train configurations at design speed across a range of bearing stiffnesses to determine rotordynamic feasibility. The key learning indicates two of the five configurations could be used for future refinement.

ACKNOWLEDGEMENTS

The authors would like to acknowledge the support and contributions of the US Department of Energy (DoE) under contract DE-EE0010318. Special thanks to our partners at SwRI and Sandia National Laboratory for their collaboration and insights. Additionally, we appreciate the efforts of the research team at GE Vernova Advanced Research, Christopher Easterby, Joseph Cotroneo, Jason P. Mortzheim for their dedication and hard work in advancing sCO2 technology.

DISCLAIMER

REFERENCES

[1] C. K. Ho, J. N. Sment, K. J. Albrecht, B. M. Mills and N. Schroeder, "Gen 3 Particle Pilot Plant (G3P3) -- High-Temperature Particle System for Concentrating Solar Power (Phases 1 and 2)," Sandia National Laboratories, Albuquerque, NM, 2021.

[2] Southwest Research Institute, "DE-EE0005804: Development of a High Efficiency Hot Gas Turboexpander and Low Cost Heat Exchangers for Optimized CSP Supercritical CO2 Operation," Southwest Research Institute, San Antonio, TX, 2017.

[3] National Energy Technology Laboratory, "STEP 10 MWe Pilot Plant," [Online]. Available: https://netl.doe.gov/carbon-management/sco2/step10pilotplant. [Accessed 11 November 2025].

[4] J. Mortzheim, "Compression System Design and Testing for sCO2 CSP Operation," General Electric, Niskayuna, NY, 2019.

[5] U.S. Department of Energy, "SETO 2020 – Integrated TESTBED – Heliogen, Inc.," [Online]. Available: https://www.energy.gov/eere/solar/seto-2020-integrated-testbed-heliogen-inc?nrg_redirect=371934. [Accessed 11 November 2025].

[6] R. Buck and S. Giuliano, "Solar Tower System Temperature Range Optimization for Reduced LCoE," in *SolarPACES 2018 AIP Conf. Proc. 2126, 030010-1–030010-8; https://doi.org/10.1063/1.5117522*, 2021.

[7] J. Mortzheim, D. Hofer, S. Priebe, A. McClung, J. J. Moore and S. Cich, "Challenges With Measuring Supercritical CO2 Compressor Performance When Approaching the Liquid-Vapor Dome," in *ASME Turbo Expo 2021: Turbomachinery Technical Conference and Exposition*, 2021.

[8] S. Pierre, Y. Chiu, G. Jothiprasad and J. Moore, "Performance Predictions for a Super-Critical CO2 Compressor Operating Near the Liquid-Vapor Dome," in *Proceedings of ASME Turbo Expo 2025 Turbomachinery Technical Conference and Exposition GT2025*, Memphis, TN, 2025.

[9] J. Marion, M. Kutin, A. McClung, J. Mortzheim and R. Ames, "The STEP 10 MWe sCO2 Pilot Plant Demonstration," in *Proceedings of ASME Turbo Power Expo 2022 Turbomachinery Technical Conference and Exposition*, Rotterdam, Netherlands, 2022.

[10] R. Bidkar, G. Anil, M. Musgrove, T. Day, A. A. Maxwell, D. Peter, C. Hofer and J. Moore, "Conceptual Designs of 50 MWe and 450 MWe Supercritical CO2 Turbomachinery Trains for Power Generation from Coal. Part 1: Cycle and Turbine," in *The 5th International Symposium - Supercritical CO2 Power Cycles* , San Antonio, TX, 2016.

[11] B.Ertas, J.Zierer, A.McClung, D.Torrey and R.A.Bidkar, "Super-Critical Carbon Dioxide Power Cycle For Waste Heat Recovery Utilizing Hermetic Oil-Free Turbomachinery: Cycle and Conceptual Turbomachinery Design," in *GT2023-104245*, Boston, MA USA, 2023.

[12] C.K.Ho, "energy.gov," September 2021. [Online]. Available: https://www.energy.gov/sites/default/files/2021-09/Ho_G3P3%20Overview_SNL.pdf.

[13] "energy.gov," 05 March 2021. [Online]. Available: https://www.energy.gov/eere/solar/generation-3-concentrating-solar-power-systems-gen3-csp.

[14] *ASPEN PLUS V14,* Burlington, MA: ASPEN Technology Inc., 2024.

[15] "conceptsnrec.com," [Online]. Available: https://www.conceptsnrec.com/compressor-design-software.

[16] E. Lemmon, I. Bell, M. Huber and M. McLinden, "NIST Standard Reference Database 23: Reference Fluid Thermodynamic and Transport Properties-REFPROP, Version 10.0," National Institute of Standards and Technology, Gaithersburg, 2018.

[17] O. E. Balje, ""A Study on Design Criteria and Matching of Turbomachines: Part A—Similarity Relations and Design Criteria of Turbines"," *ASME. J. Eng. Power,* vol. 81, pp. 83-102, 1962.

[18] O. E. Balje, "A Study on Design Criteria and Matching of Turbomachines: Part B—Compressor and Pump Performance and Matching of Turbocomponents," *ASME Journal of Engineering for Power,* vol. 84, pp. 103-114, 1962.

[19] A. J. Glassman and W. L. Stewart, "Use of Similarity Parameters for Examination of Geometry Characteristics of High-Expansion-Ratio Axial-Flow Turbines," NASA Technical Note: D-4248, Cleveland, OH, 1967.

[20] X.Ziyuan, Y.Yang, S.Mao, W.Wu and Q.Yang, "Review on corrosion of alloys for application in supercritical carbon dioxide brayton cycle," *Heliyon,* vol. 9, no. 11, 2023.

[21] J.E.Vrancik, "Prediction of Windage Power Loss in Alternators," NASA TN D-4849, Cleveland, Ohio, 1968.

[22] "dyrobes.com," [Online]. Available: https://dyrobes.com.

Dr. Amin Changizi received his Ph.D. degree from Concordia University, Canada. He is currently a Senior Research Mechanical Engineer with GE Vernova Advanced Research Center. He is working on turbomachine designs. He was with different industries like Plug Power, MITI, Carrier Corporation. Prior to that, he was a part time faculty member with Concordia University. He has been a full-time faculty member for several years, and an engineer in various positions within the pump industry. His research interests are turbomachines, rotodynamic, theoretical nonlinear mechanics, Lie symmetry method with applications on nonlinear differential equations, and nonlinear behaviors of MEMS devices.

Mr. Sylvain Pierre is a Senior Engineer in the Aerodynamics & Thermal Sciences Lab at GE Vernova Advanced Research in Niskayuna, NY. He has over 35 years of gas turbine design and development test experience for commercial aviation and power generation industries. His current research interests include turbomachinery aerodynamics, advanced closed power cycles, transonic and supersonic flow physics and controls. He currently holds 15 patents, and received his M.Eng. from McGill University, Canada.

Dr. Yuankang Chen is a Research Engineer in the Power Systems group at the GE Vernova Advanced Research Center in Niskayuna, NY. He received his PhD in Aeronautics and Astronautics from MIT, with a technical background in multidisciplinary design and analysis of high-speed electric machines. His research interests include advanced electric machine designs for power and propulsion, turbo-electric integration, and high power-density power electronics.

Dr. Daniel Bacellar has over 15 years of experience in the Energy sector, with emphasis in thermal fluid technologies. He holds a Ph.D. in Mechanical Engineering from the University of Maryland, College Park, where he also had a non-tenured faculty appointment as assistant research professor. Dr. Bacellar has a strong technical background with experience in academia, consulting, and industry. He is currently a Lead Engineer in the Aerodynamics & Thermal Sciences group within GE Vernova Advanced Research.

Dr. Thomas Mancuso is a Senior Engineer in the Aerodynamics & Thermal Sciences Lab at GE Vernova Advanced Research in Niskayuna, NY. He has 34 years' experience in the thermal-fluids engineering. He received his PhD from Michigan Tech, his Master's degree from Virginia Tech and his Bachelor's degree from Penn State, all in Mechanical Engineering. His research interest includes turbomachinery and electric machine cooling, cryogenics and CFD.